Exploring the limits of existence of proton-rich nuclei in the $Z = 70$–82 region

E. M. Lykiardopoulou,[1,2] G. Audi,[3] T. Dickel,[4,5] W. J. Huang,[6,3] D. Lunney,[3] Wolfgang R. Plaß,[5,4] M. P. Reiter,[7] J. Dilling,[1,2] and A. A. Kwiatkowski[1,8]
(TITAN Collaboration)
[1]*TRIUMF, 4004 Wesbrook Mall, Vancouver, British Columbia V6T 2A3, Canada*
[2]*Department of Physics and Astronomy, University of British Columbia, Vancouver, British Columbia V6T 1Z1, Canada*
[3]*Université Paris-Saclay, CNRS/IN2P3, IJCLab, 91405 Orsay, France*
[4]*GSI Helmholtzzentrum für Schwerionenforschung GmbH, 64291 Darmstadt, Germany*
[5]*II. Physikalisches Institut, Justus-Liebig-Universität, 35392 Gießen, Germany*
[6]*Advanced Energy Science and Technology Guangdong Laboratory, Huizhou 516007, China*
[7]*School of Physics and Astronomy, University of Edinburgh, Edinburgh EH9 3FD, United Kingdom*
[8]*Department of Physics and Astronomy, University of Victoria, Victoria, British Columbia V8P 5C2, Canada*

(Received 13 September 2022; accepted 3 February 2023; published 21 February 2023; corrected 1 February 2024)

α-, β-, and proton-decay energies have been combined with TITAN mass values for $^{150-157}$Yb to expand and refine the mass surface in the proton-rich $Z = 70$–82 region. The calculations were performed using the Atomic Mass Evaluation (AME) algorithm, resulting in 11 new ground-state masses and uncertainty reductions of nine others. The new information allows the determination of the two-proton drip line for elements between Ir and Pb and provides indications of possible new candidates for two-proton emission. In addition, we examined binding energies in this region for Thomas-Ehrman shifts, so far only visible for light nuclides.

DOI: 10.1103/PhysRevC.107.024311

I. INTRODUCTION

A stringent test of a global nuclear theory is the prediction of the number of bound nuclides, determined from neutron and proton emission, in addition to spontaneous fission [1]. The limits to the nuclear chart are defined by the so-called driplines, beyond which no additional neutron or proton can be added to the nucleus. Except for lighter systems, the neutron dripline extends to isotopes located well beyond what is reachable experimentally, whereas the proton dripline is located much closer to stability, due to Coulomb-repulsion effects that grow with increasing atomic number, Z. The process of proton emission [2] is therefore intriguing since it can be energetically possible and experimentally within reach. Ground-state proton emission, first observed from ^{151}Lu [3] and ^{147}Tm [4] in 1982, is now known to occur in over 50 cases. Rarer is the process of two-proton decay [5], first seen from ^{45}Fe only 20 years ago [6,7] and the recent spectacular observation of sequential $2p$ decays from ^{18}Mg, via ^{16}Ne to ^{14}O [8]. Two-proton decay has now been observed up to ^{67}Kr ($Z = 36$) [9] and gives unique information about the exotic parent nuclide.

Finding heavier candidates for two-proton decay requires, among other properties [5], knowledge of the mass surface at the dripline, since it is the binding energy that determines the amount of energy available for nuclear decay. Already for $A > 100$ proton decay is in strong competition with α decay, which is also the case below the $Z = 82$ shell closure. Novikov *et al.* [10] describe this peculiar region as the "littoral shallow", where nuclides are proton unbound but do not emit protons due to the large Coulomb barrier that slows the tunneling process and allows them to β (or α) decay instead.

In addition to the discovery of candidates for two-proton emission, knowledge of the mass surface can probe exotic phenomena such as the existence of the Thomas-Ehrman shift [11]. Since it was discovered, in the 1950s in ^{13}C and ^{13}N [12,13], the Thomas-Ehrman shift has been repeatedly measured in light systems [11], but it has never been observed in heavy nuclei [10,14].

In general, binding energies or masses are either determined from reactions and decays or directly by mass spectrometry. Currently, for heavier nuclides near the proton dripline, α decay is the dominant source, however only mass differences are obtained. Unless the mass of at least an α-decay daughter nucleus is known, none of the decay energies can be linked to the mass surface (also true for β decay). Moreover, α decay follows a path that is less than parallel to the proton dripline, thwarting the mass determination of more exotic nuclides. Mass spectrometry can provide a complementary solution if one of the nuclides in the chain can be measured.

The combination of reaction, decay, and mass spectrometric data obtained worldwide is performed periodically within the Atomic Mass Evaluation (AME), and leads to the table of atomic masses. The most recent publication AME2020 [15] includes several α-decay chains for which the masses were extrapolated since no links to known masses existed.

Considering all the known decay energies, a reaction network can be constructed, where the known α-reaction

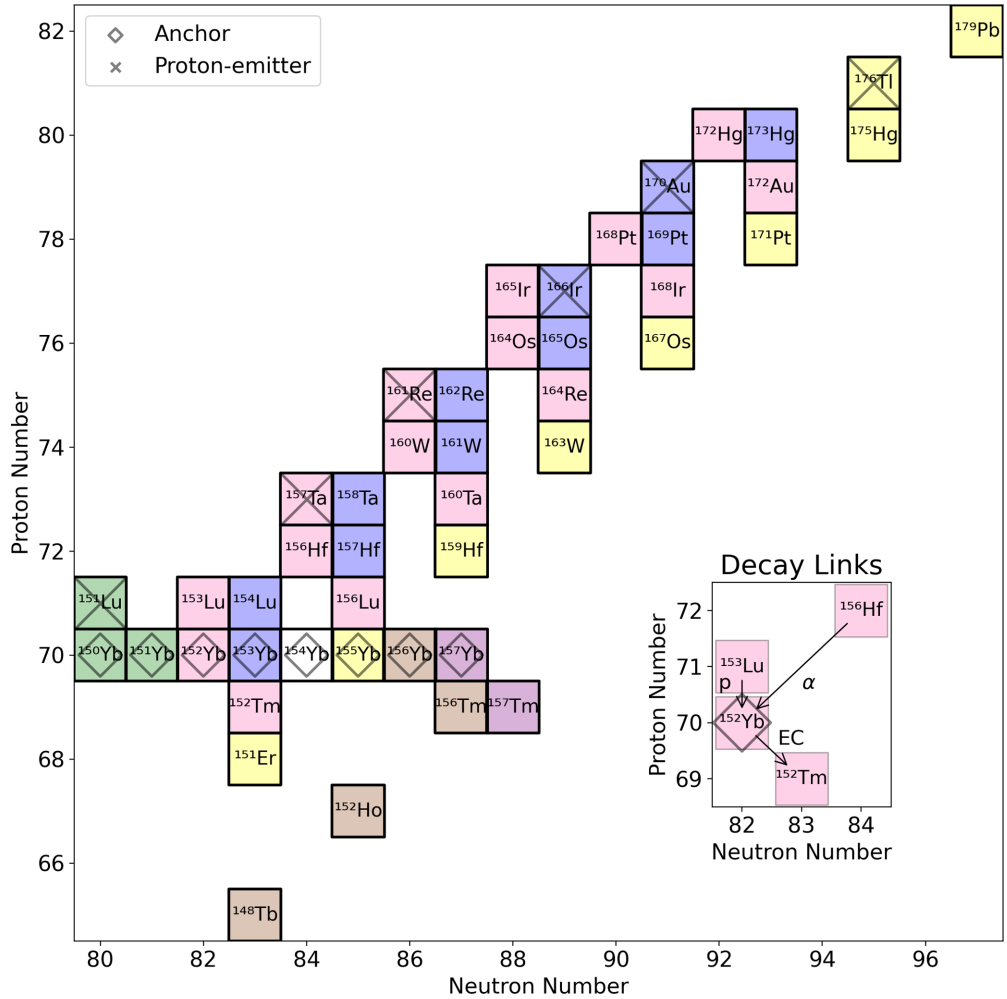

FIG. 1. Connection diagram of all isotopes determined in this work; all isotopes that share the same color (chains) are connected by known Q_α, Q_β, or S_p. The masses of these isotopes are determined using known decay energies and the AME algorithm. The anchors of the chains are represented with diamonds, while the one-proton emitters are marked with x symbols. The insert shows an example of how nuclei link to ^{152}Yb.

and proton-separation energies can be expressed as mass differences. However, the masses themselves cannot be determined unless at least one mass in the network is experimentally determined. We refer to the experimentally determined mass as the anchor, since it has the property of anchoring the masses of all nuclides linked in the network. This, in turn, allows the calculation of proton binding over a large number of proton and neutron numbers, which is extremely challenging to measure directly.

Using TRIUMF's Ion Trap for Atomic and Nuclear science (TITAN) [16], we recently measured the masses of neutron-deficient isotopes $^{150–157}$Yb ($Z = 70$) [17] with the TITAN MR-ToF MS [18]. Experimental details of the operation of the device can be found in [19]. These masses anchor a number of α chains in the $Z = 70$–82 region [20] and therefore give information about the topology of the shore, revealing possible proton emitters that allow us to wade in the sea of instability and explore the littoral shallow.

In the following section we describe the AME procedure for anchoring these decay chains and present the new mass values, before examining the updated mass surface in Sec. III and searching for signs of the Thomas-Ehrman shift [11] in Sec. IV.

II. CALCULATION PROCEDURE

In the framework of the Atomic Mass Evaluation (AME) algorithm [21] the nuclear chart is represented as a reaction network. Depending on how many connections are used to determine the mass of a nuclide, each nuclide is categorized as primary (with multiple connection links) or secondary (with a single connection link). Anchoring several nuclides belonging to an α chain to other primary nuclides therefore transforms the member masses from unknown into primary.

As can be seen in Fig. 1, the measured Yb isotopes (marked with diamonds) are connected via known α, β, and proton decay energies to nuclides that reach as far as ^{179}Pb ($Z = 82$). The Yb mass values that contributed significantly in reducing uncertainties and determining other unmeasured masses were those of ^{150,152,153}Yb. The ground-state mass-excess values and isomeric energies calculated from the five anchors can be

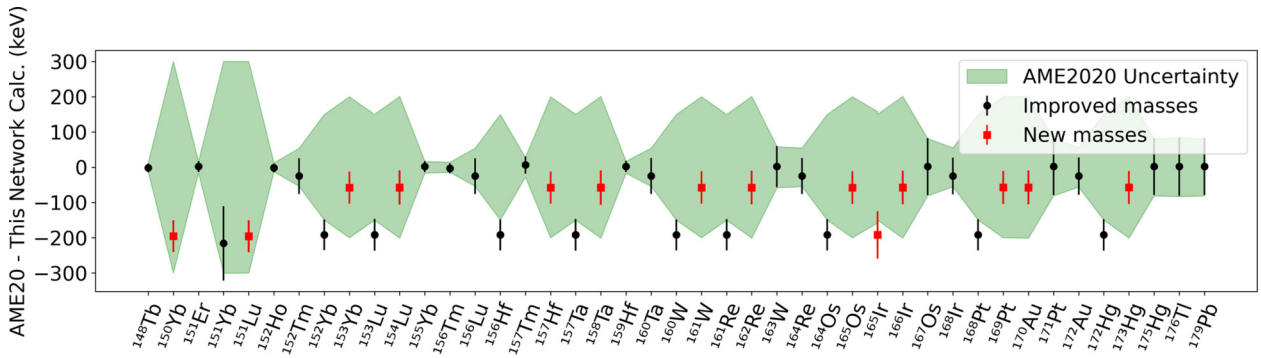

FIG. 2. Comparison between AME2020 and the masses determined in this work. The green area indicates the AME2020 uncertainty. Nuclides with similar deviations belong to a common α chain and their deviation arises from the deviation in the mass of the α chain anchor.

seen in Table I and the deviation between the ground state masses and their AME2020 values is depicted in Fig. 2.

The AME algorithm can be depicted as a network of interconnected nuclei, where their masses are linked by the experimentally measured decays. In this work, and in accordance with [21], we entered the new masses in the form of mass ratios $R = m_{\rm ion}/m_{\rm ion}^{\rm cal}$, where $m_{\rm ion}$ the mass of the ion measured with the TITAN MR-TOF-MS and $m_{\rm ion}^{\rm cal}$ is the mass of an isobaric calibrant ion observed in the same mass spectrum. The advantage of this format is that any subsequent change in the mass of the calibrant ion is automatically incorporated in the future mass evaluations. The entered ratios are then converted to linear equations of masses of neutral atoms according to the recipe described in Ref. [21] and the primary masses are adjusted by solving the equation

$$\mathbf{K}\,|m\rangle = |E\rangle \tag{1}$$

using the least-squares minimization method. In Eq. (1), $\mathbf{K}$ is the connectivity matrix, $|m\rangle$ are the masses that are being adjusted, and $|E\rangle$ is the array of the decay energies.

In the neutron deficient side of the nuclear chart, the connectivity matrix $\mathbf{K}$ is constructed from known α decays, proton-separation energies as well as β decays/ Electron Captures (EC):

$$m(Z,A) - m(Z-2,A-4) = Q_\alpha/c^2 + m(^4\mathrm{He}), \tag{2}$$

$$-m(Z,A) + m(Z-1,A-1) = S_p/c^2 - m(^1\mathrm{H}), \tag{3}$$

$$-m(Z,A) + m(Z-2,A-2) = S_{2p}/c^2 - 2m(^1\mathrm{H}), \tag{4}$$

$$m(Z,A) - m(Z-1,A) = Q_{\rm EC}/c^2. \tag{5}$$

As an example, two of the nuclides that were used as an input to the AME algorithm in this work were ^{150,151}Yb. Both of them can be used to determine the mass of the parent ^{151}Lu through the decays

$$^{151}\mathrm{Lu} \rightarrow {}^{150}\mathrm{Yb} + p \tag{6}$$

and

$$^{151}\mathrm{Lu} + e^- \rightarrow {}^{151}\mathrm{Yb} + \nu_e. \tag{7}$$

With the aid of the known decay energies $S_p \pm \delta S_p$ and $Q_{EC} \pm \delta Q_{EC}$, the mass of ^{151}Lu can be adjusted by solving Eq. (1) for the two decays

$$\begin{bmatrix} -1 & 1 & 0 & 1 & 0 \\ 1 & 0 & -1 & 0 & 0 \end{bmatrix} \begin{bmatrix} m_{^{151}\mathrm{Lu}} \\ m_{^{150}\mathrm{Yb}} \\ m_{^{151}\mathrm{Yb}} \\ m_{^{1}\mathrm{H}} \\ m_{^{4}\mathrm{He}} \end{bmatrix} = \begin{bmatrix} S_p \pm \delta S_p \\ Q_{\rm EC} \pm \delta Q_{\rm EC} \end{bmatrix}.$$

A complete connection network involving all Yb isotopes presented in this work can be constructed in the same way. More detailed information about the AME algorithm can be found in Ref. [15].

A schematic of the complete connection network concerning this work can be seen in Fig. 1. For simplicity, only the isotopes whose mass uncertainty was improved in this work are depicted in the figure. Isotopes with the same color represent groups that are linked by either α or proton or β decay (an example is illustrated in the inset of Fig. 1).

In total, the anchors ^{152,153,155,156}Yb give access to seven different α chains as can be seen in Fig. 1. Both the α chains anchored to ^{152,153}Yb are interlinked with two other α chains via the proton emitters ^{157}Ta, ^{161}Re, and ^{166}Ir and ^{170}Au, respectively. The masses in the α chain involving ^{152}Yb have previously been determined with a precision of 150 keV [15] while the ones in the α chain of ^{153}Yb have never been determined before. In total, considering all the Yb isotopes entered in the connection network, we were able to determine the mass of 11 new ground states and improve the precision of nine other ground-state masses by more than a factor of 2 in the region between $Z = 71$ and $Z = 82$. The adjusted mass excess ME $= m(Z,A) - A$ values of all isotopes determined in this work are listed in Table I. Due to a 200 keV deviation between the previous mass value for ^{152}Yb and the TITAN measurement, the masses of all isotopes in the chain anchored by ^{152}Yb have been shifted by $\approx$200 keV, as can be seen in Fig. 2. Overall, our results are in agreement with the 2020 Atomic Mass Evaluation [15].

III. SEPARATION ENERGIES AND THE TWO-PROTON DRIPLINE

The one and two-proton separation energies were calculated from the ME values of Table I. The one-proton separation energy, S_p, defined in Eq. (3), expresses the energy

TABLE I. The mass excess (ME) of the isotopes determined in this work and their corresponding ME from AME2020. The last four columns contain the one (S_p) and two-proton separation energies (S_{2p}) as calculated from the ME values determined in this work. The calculated S_p and S_{2p} only consider transitions between ground states. The anchors that were used in this study from [17] are noted with an asterisk while values accompanied by the # symbols in the columns $ME_{AME2020}$ and its uncertainty (unc.) represent AME2020 extrapolations [15].

Isotope	ME (keV)	unc. (keV)	$ME_{AME2020}$ (keV)	unc. (keV)	S_p (keV)	unc. (keV)	S_{2p} (keV)	unc. (keV)
^{148}Tb	−70535	12	−70537	12	2467	13	7995	14
^{150}Yb*	−38635	45	−38830#	300#	1983	205	1733	46
^{151}Er	−58268	15	−58266	17	3611	21	5152	18
^{151}Yb*	−41326	106	−41542	300	2124	222	2162	109
^{151}Yb^{m}*	−40617	49						
^{151}Lu	−30105	45	−30300#	300#	−1241	64	742	205
^{151}Lu^{m}	−30048	45	−30244#	300#				
^{152}Ho	−63603	12	−63605	13	2139	13	7074	14
^{152}Tm	−51695	51	−51720	54	716	53	4327	53
^{152}Yb*	−46079	44	−46270	150	2596	48	2825	47
^{153}Yb*	−47102	46	−47160#	200#	2696	68	3412	48
^{153}Lu	−38184	45	−38375	150	−606	63	1990	49
^{153}Lu^{m}	−38104	45	−38296	150				
^{154}Lu	−39609	48	−39667#	201#	−204	66	2492	70
^{154}Lu^{m}	−39547	48	−39604#	201#				
^{155}Yb*	−50505	16	−50503	17	3366	21	4616	18
^{156}Tm	−56831	14	−56834	14	1911	15	6770	16
^{156}Lu	−43675	51	−43700	54	459	53	3825	53
^{156}Hf	−37628	44	−37820	150	2371	48	2273	47
^{156}Hf^{m}	−35669	44	−35861	150				
^{157}Tm	−58716	24	−58709	28	1793	34	7253	30
^{157}Hf	−38797	46	−38855#	200#	2412	68	2871	48
^{157}Ta	−29404	45	−29596	150	−935	63	1437	49
^{157}Ta^{m}	−29382	45	−29574	150				
^{157}Ta^{n}	−27811	45	−28003	150				
^{158}Ta	−31061	48	−31118#	201#	−448	66	1964	70
^{158}Ta^{m}	−30919	48	−30977#	201#				
^{158}Ta^{n}	−28253	49	−28311#	201#				
^{159}Hf	−42855	16	−42853	17	2931	22	4012	19
^{160}Ta	−35799	51	−35824	54	233	53	3164	53
^{160}W	−29137	44	−29329	150	1987	48	1613	47
^{161}W	−30449	46	−30507#	200#	1940	69	2178	49
^{161}Re	−20651	44	−20843	150	−1197	62	790	48
^{161}Re^{m}	−20527	44	−20719	150				
^{162}Re	−22395	47	−22453#	201#	−765	66	1175	70
^{162}Re^{m}	−22220	48	−22278#	201#				
^{163}W	−34910	58	−34908	58	2418	86	3172	63
^{164}Re	−27447	51	−27472	55	−174	78	2244	81
^{164}Os	−20233	44	−20425	150	1519	48	811	48
^{165}Os	−21689	46	−21747#	200#	1531	69	1357	74
^{165}Ir	−11403#	67#	−11595#	158#	−1541	80	−21	70
^{165}Ir^{m}	−11223	45	−11415	150				
^{166}Ir	−13248	47	−13306#	201#	−1152	66	379	70
^{166}Ir^{m}	−13077	48	−13134#	201#				
^{167}Os	−26501	81	−26499	81	1952	120	2217	85
^{168}Ir	−18641	52	−18666	55	−571	96	1382	102
^{168}Pt	−10818	44	−11010	150	1035	48	−35	48
^{169}Pt	−12407	47	−21464#	200#	1054	70	484	93
^{170}Au	−3646	48	−3703#	201#	−1472	67	−417	71
^{170}Au^{m}	−3366	47	−3424#	201#				
^{171}Pt	−17469	81	−17467	81	1575	130	1323	85
^{172}Au	−9293	53	−9318	56	−886	97	689	115
^{172}Hg	−869	45	−1061	150	596	49	−852	48
^{173}Hg	−2604	47	−2661#	201#	600	71	−287	93
^{175}Hg	−7971	81	−7969	81	1202	130	613	103
^{176}Tl	583	83	585	83	−1265	116	−63	131
^{179}Pb	2050	81	2052	81	626	131	−247	117

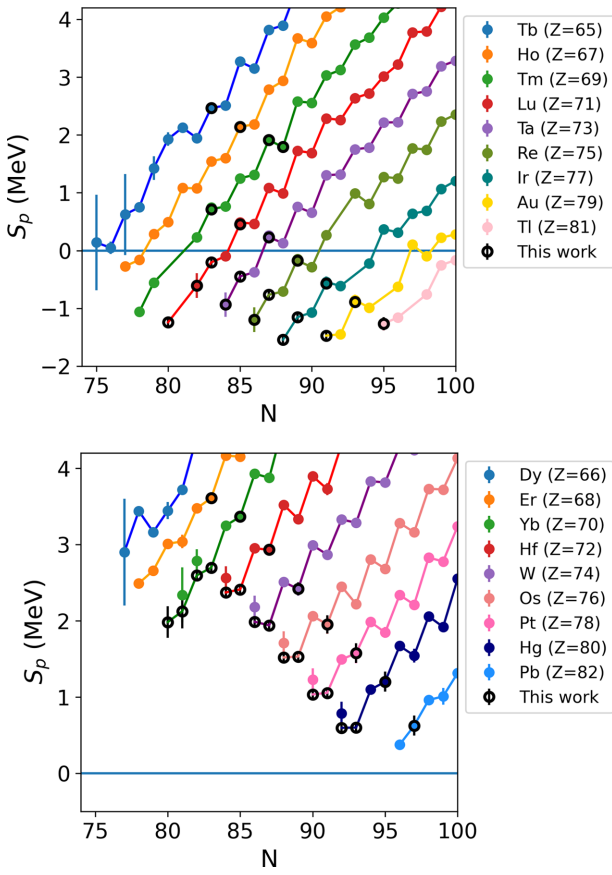

FIG. 3. One-proton separation energy as a function of neutron number N for odd-Z nuclei (top) and even-Z ones (bottom). The results of this work are represented with black data points while all other data points were calculated using the AME2020. All the data points have been calculated using existent or new masses and Eq. (3).

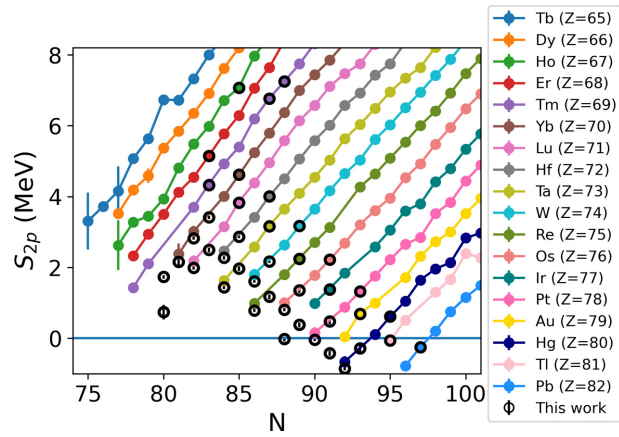

FIG. 4. Two-proton separation energy as a function of neutron number N for elements of atomic numbers $Z = 65$–82. The results of this work are represented with black data points while all other data points were calculated using the AME2020.

required to remove one proton from the nucleus and its trend can be seen in Fig. 3 for several isotopic chains. The top of Fig. 3 shows odd-Z nuclides while the bottom contains the even-Z ones. The results of this work are represented in black empty circles, while the colored data-points represent one-proton separation energies calculated from AME2020 masses [15].

The two-proton separation energy, S_{2p}, defined in Eq. (4), expresses the energy associated with the emission of two protons from the nuclide (Z, A). Positive two proton separation energy indicates bound nuclei, while negative two proton separation energy reveals the two-proton unbound nuclei. The trend of the two-proton separation energy as a function of the neutron number N is plotted in Fig. 4. Values calculated from AME2020 are depicted in colored data points connected with solid lines while the results of this work are depicted in black data points. Isotopes with $S_{2p} < 0$ are unbound to two-proton decay and thus, potential two-proton emitters provided they have $S_p > 0$.

Figure 5 places the newly calculated masses on the nuclear chart. Those that have $S_{2p} > 0$ are depicted in red while those with $S_{2p} < 0$ are depicted in blue. In total, we have found seven nuclei whose S_{2p} value is equal or smaller than zero. Out of these, ^{173}Hg, ^{170}Au, ^{165}Ir are newly found two-proton unbound nuclei that were not measured before this work. Among the other two-proton unbound nuclides, we were able to reduce the mass uncertainties of ^{172}Hg and ^{168}Pt by a factor of 3. As can be seen on the right side of Fig. 5, each color represents a range of two-proton separation energies, thus giving a perspective of the shore and the "littoral shallow" in the region.

The nuclei with $S_{2p} < 0$ and $S_p > 0$ are ^{172,173}Hg, ^{168}Pt, and ^{179}Pb, with respective half-lives 231(9) μs [22], 0.80(8) ms [23], 2.02(10) ms [24–27], and $3.5^{+1.4}_{-0.8}$ ms [28]. For all of them, α decays have been observed and their α decay branching ratios are given to be almost 100%. Though these nuclei could potentially be candidates for two-proton emission, their large Coulomb barrier would require significantly larger Q values than those of known two-proton emitters. Given that the Q_{2p} values calculated in this work are comparable with those of light two-proton emitters, although there is a finite probability for $2p$ decay, the partial half-life is too long for the decay to be experimentally observable.

The position of the drip-line as well as masses and separation energies are some of the most common quantities derived from nuclear theory calculations. It has also been repeatedly observed that different nuclear models tend to disagree by several MeV depending on their nature or their fitted parameters [1]. Experimental efforts and works, like the present one, can support and benchmark theories as well as point towards required improvements.

In the region of medium-heavy, midshell nuclei, nuclear theory calculations are performed using the mean-field framework [31]. In this framework there are two dominant branches; one that uses Skyrme interactions [32] and one that employs the Gogny force [30]. In both cases, the Hartree-Fock-Bogoliubov equations are numerically solved to provide nuclear properties such as binding energies and nuclear charge radii.

However, mean-field approaches, both in the framework of Skyrme interactions and that of Gogny forces, struggle

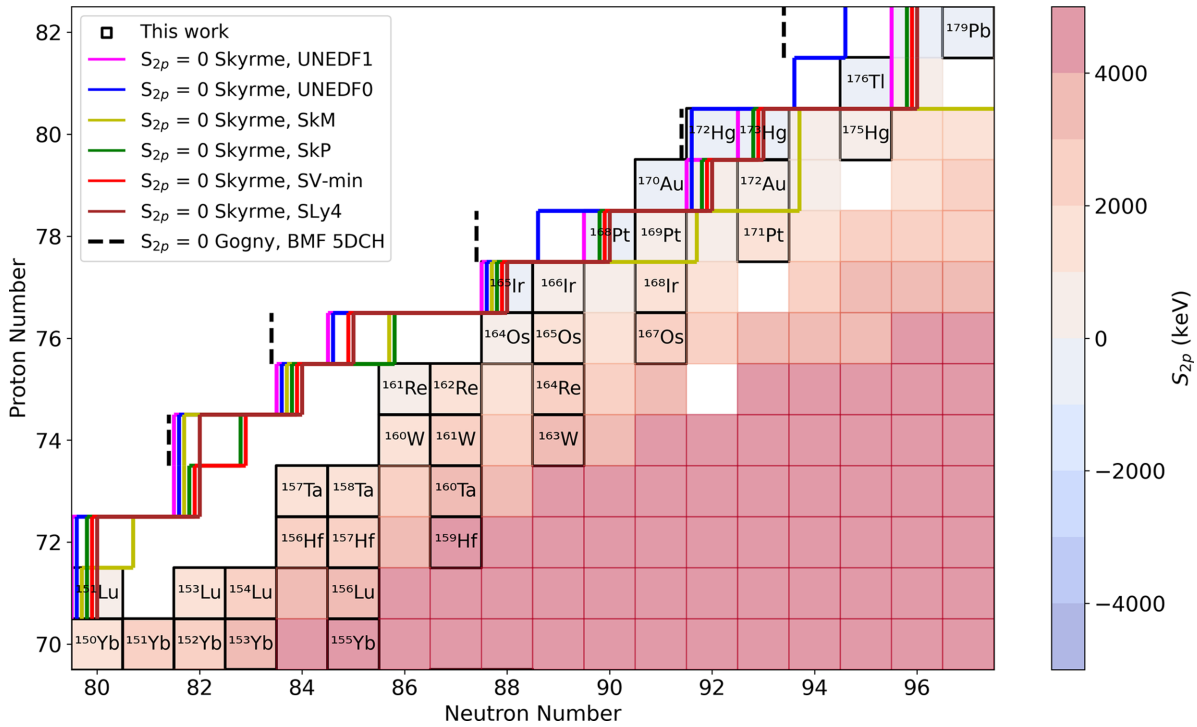

FIG. 5. Nuclear chart plot of the region between Yb and Pb. The color code indicates the two proton separation energies of the isotopes from the latest Atomic Mass Evaluation and from this work. The dark squares indicate isotopes the masses of which were determined in this work. The theoretical two-proton driplines [1,29,30] are plotted with solid and dashed lines.

to capture exotic phenomena such as deformation, while at times over- or mispredict closed shells [17]. To overcome this limitation, corrections beyond the mean field have been implemented to the model Hamiltonians. The beyond the mean-field version of the Skyrme-interaction models is encapsulated in the UNEDF0 and UNEDF1 parametrizations [32] while for the Gogny forces, the beyond mean-field approach is achieved in the CHFB+5DCH implementation [30].

We used the aforementioned models as well as other existent models based on the Skyrme interaction (SkMc[33], SkPc[34], SLy4c[35], SV-minc[36]), to locate the position of the two-proton dripline between $Z = 70$–82 and compared it to our calculated two-proton dripline. The positions of the theoretical driplines are indicated with solid and dashed lines in Fig. 5. Among the models, SkM seems to underpredict stability while the opposite is true for the Gogny BMF 5DCH model and the Skyrme UNEDF0.

IV. THOMAS-EHRMAN SHIFTS

In the early 1950s, Thomas [12] and Ehrman [13] discovered that there is a shift in the expected Coulomb energies between ^{13}C and ^{13}N. This shift was later named after them and it has been repeatedly measured in light proton-unbound systems [11]. Its origin comes from the fact that when a proton is loosely bound to the nucleus, the overlap of its wave function and that of the rest of the nucleus is reduced and therefore the Coulomb repulsion is weaker. It has also been found that this effect is more prominent in light nuclei where the Coulomb barrier is small and for nuclei with low angular momentum quantum numbers where the centrifugal potential is not too strong [11]. The Thomas-Ehrman shift is thought to (partially) explain the reduced $N = 8$ shell effect in the four-proton-unbound ^{18}Mg result [8].

In the low-mass region of the nuclear chart, the study of Thomas-Ehrman shifts has focused on using mirror nuclei. However, for $Z > 50$ no known mirror nuclei exist. Novikov *et al.* [10] therefore took a different approach, assuming if there is a shift in the Coulomb energies of the proton-unbound nuclei, the trend of one-proton separation energy should change across the dripline. Using the binding energy as phenomenologically described by the semiempirical mass formula

$$\mathrm{BE} = \alpha_V A - \alpha_S A^{2/3} - \alpha_C \frac{Z(Z-1)}{A^{1/3}} \tag{8}$$

$$-\alpha_A \frac{(N-Z)^2}{A} + \delta(N,Z),$$

they expressed the one-proton separation energy as

$$S_p = \alpha + \beta A^{-1/3} + \gamma A^{-1}, \tag{9}$$

where α, β, γ are fit parameters. In their approach they only fitted the bound nuclei close to the proton drip-line, extrapolated and looked for deviations between the extrapolated line and the measured unbound nuclei.

In this work, starting from the linearity of S_p as a function of A when there are no significant changes in nuclear structure (shell closures, deformation, etc.), we choose to simplify the

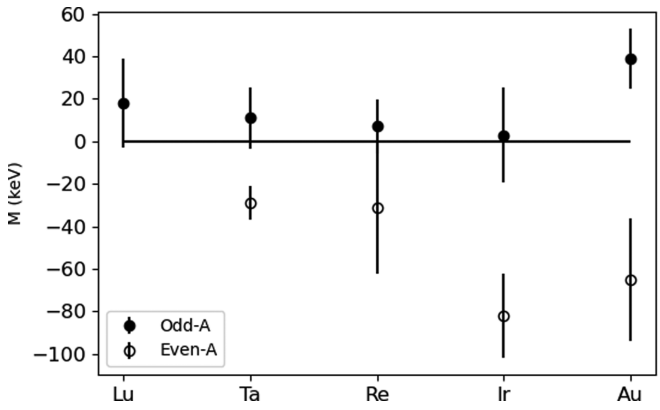

FIG. 6. Plot of the metric M for different isotopic chains. All values above zero correspond to fits for odd-A nuclei while all the ones below zero correspond to even-A ones. For the linear fit of even-A Ta, Ir, and Au, only two S_p values were available for each case.

fit further and we define our fitting function as

$$S_p = aA + b, \tag{10}$$

where a, b are the fit parameters. Using the PYTHON least-square Statsmodels module [37], we fit Eq. (10) separately for proton-bound and proton-unbound nuclides. After obtaining the slopes a and their uncertainty δa for the bound and unbound data sets, we define a metric indicating a possible kink between proton-bound and proton-unbound fitted lines that would reveal a Thomas-Ehrman shift:

$$M = a_+ - a_-, \tag{11}$$

where a_+ and a_- are the slopes of the proton-bound and proton-unbound nuclides, respectively.

From the data obtained in this work we only investigated the existence of Thomas-Ehrman shifts in odd-Z nuclei since their one-proton drip-line is within reach. We also used one-proton separation energies calculated in this work and included AME2020 values when needed.

The results can be seen in Fig. 6 for each of the odd-Z elements; Lu, Ta, Re, Ir, and Au. The error bars correspond to the uncertainties δM_+ and δM_- added quadratically. For Lu there is no result for even-A nuclei because there is only one Lu isotope with known S_p and therefore there are insufficient data points for a fit. In addition, we note that the results for even-A Ta, Ir, and Au isotopes are based on a two-point linear fit as in each of the three cases there are only two proton-unbound isotopes available.

Based on the results depicted in Fig. 6, there is a slight but noticeable (2σ) discrepancy in the slope of proton-bound and proton-unbound odd-A Au isotopes, which could be a result of a Thomas-Ehrman shift. In addition, the presence of Thomas-Ehrman shifts for Au nuclei agrees with the expectation that odd-A, proton-unbound Au isotopes with low spin ($J^\pi = 1/2^+$) are more likely to show shifts compared to higher spin isotopes like the odd-A, proton-unbound Lu isotopes ($J^\pi = 11/2^-$) or the even-A Re isotopes ($J^\pi = 2^-$). However, measurements of more proton-unbound isotopes of the mentioned species are required for a conclusive result.

V. CONCLUSION

We used mass measurements of $^{150–157}$Yb isotopes as anchor points for long decay chains which resulted in 11 new ground state mass values as well as improvements of nine other ground state masses by at least a factor of 2. Exploring the mass surface by calculating the two-proton separation energies from the determined masses, we located the two-proton drip-line between $Z = 77$ and 82, and show that the newly determined ^{168}Pt, ^{172,173}Hg, and ^{179}Pb could be candidates for two-proton emission, although the partial half-lives are likely too long, thus making α decay the most promising decay type. Comparison with theoretical works shows that Skyrme interactions tend to predict the two proton drip-line with relative accuracy, for the region of interest without taking into consideration theoretical uncertainties. Finally, we used the calculated masses to determine one-proton separation energies and investigated the presence of Thomas-Ehrman shifts in the odd-Z nuclei of this work, finding a possible occurrence in the odd-A, proton-unbound Au isotopes although more data on proton-unbound nuclei are needed before drawing a definite result.

ACKNOWLEDGMENTS

The authors would like to thank Yu. Novikov for the fruitful discussions towards Thomas-Ehrman shifts. This work was supported by the Natural Sciences and Engineering Research Council (NSERC) of Canada under Grant No. SAPPJ-2022-00022, the National Research Council of Canada (NRC) of Canada through TRIUMF and by the French IN2P3.

[1] J. Erler, N. Birge, M. Kortelainen, W. Nazarewicz, E. Olsen, A. M. Perhac, and M. Stoitsov, The limits of the nuclear landscape Nature **486**, 509 (2012).

[2] V. Goldansky, On neutron-deficient isotopes of light nuclei and the phenomena of proton and two-proton radioactivity, Nucl. Phys. **19**, 482 (1960).

[3] S. Hofmann, W. Reisdorf, G. Münzenberg, F. Heßberger, J. Schneider, and P. Armbruster, Proton radioactivity of 151 Lu, Z. Phys. A **305**, 111 (1982).

[4] D. Schardt, Direct proton decay of 147 Tm, *Heavy-Ion Collisions* (Springer, Berlin, 1982), pp. 256–266.

[5] B. Blank and M. Borge, Nuclear structure at the proton drip line: Advances with nuclear decay studies, Prog. Part. Nucl. Phys. **60**, 403 (2008).

[6] M. Pfützner, E. Badura, C. Bingham, B. Blank, M. Chartier, H. Geissel, J. Giovinazzo, L. V. Grigorenko, R. Grzywacz, M. Hellström, Z. Janas, J. Kurcewicz, A. S. Lalleman, C. Mazzocchi, I. Mukha, G. Mũnzenberg, C. Plettner, E. Roeckl,

K. P. Rykaczewski, K. Schmidt *et al.*, First evidence for the two-proton decay of ^{45}Fe, Eur. Phys. J. A **14**, 279 (2002).

[7] J. Giovinazzo, B. Blank, M. Chartier, S. Czajkowski, A. Fleury, M. J. Lopez Jimenez, M. S. Pravikoff, J.-C. Thomas, F. de Oliveira Santos, M. Lewitowicz, V. Maslov, M. Stanoiu, R. Grzywacz, M. Pfützner, C. Borcea, and B. A. Brown, Two-Proton Radioactivity of ^{45}Fe, Phys. Rev. Lett. **89**, 102501 (2002).

[8] Y. Jin, C. Y. Niu, K. W. Brown, Z. H. Li, H. Hua, A. K. Anthony, J. Barney, R. J. Charity, J. Crosby, D. Dell'Aquila, J. M. Elson, J. Estee, M. Ghazali, G. Jhang, J. G. Li, W. G. Lynch, N. Michel, L. G. Sobotka, S. Sweany, F. C. E. Teh *et al.*, First Observation of the Four-Proton Unbound Nucleus ^{18}Mg, Phys. Rev. Lett. **127**, 262502 (2021).

[9] T. Goigoux, P. Ascher, B. Blank, M. Gerbaux, J. Giovinazzo, S. Grévy, T. Kurtukian Nieto, C. Magron, P. Doornenbal, G. G. Kiss, S. Nishimura, P.-A. Söderström, V. H. Phong, J. Wu, D. S. Ahn, N. Fukuda, N. Inabe, T. Kubo, S. Kubono, H. Sakurai *et al.*, Two-Proton Radioactivity of ^{67}Kr, Phys. Rev. Lett. **117**, 162501 (2016).

[10] Y. Novikov, F. Attallah, F. Bosch, M. Falch, H. Geissel, M. Hausmann, T. Kerscher, O. Klepper, H.-J. Kluge, C. Kozhuharov, Y. Litvinov, K. Löbner, G. Münzenberg, Z. Patyk, T. Radon, C. Scheidenberger, A. Wapstra, and H. Wollnik, Mass mapping of a new area of neutron-deficient suburanium nuclides, Nucl. Phys. A **697**, 92 (2002).

[11] E. Comay, I. Kelson, and A. Zidon, The Thomas-Ehrman shift across the proton dripline, Phys. Lett. B **210**, 31 (1988).

[12] R. G. Thomas, An analysis of the energy levels of the mirror nuclei, ^{13}C and ^{13}N, Phys. Rev. **88**, 1109 (1952).

[13] J. B. Ehrman, On the displacement of corresponding energy levels of ^{13}C and ^{13}N, Phys. Rev. **81**, 412 (1951).

[14] K. Auranen, J. Uusitalo, H. Badran, T. Grahn, P. T. Greenlees, A. Herzáň, U. Jakobsson, R. Julin, S. Juutinen, J. Konki, M. Leino, A.-P. Leppänen, G. O'Neill, J. Pakarinen, P. Papadakis, J. Partanen, P. Peura, P. Rahkila, P. Ruotsalainen, M. Sandzelius *et al.*, Exploring the boundaries of the nuclear landscape: α-decay properties of ^{211}Pa, Phys. Rev. C **102**, 034305 (2020).

[15] M. Wang, W. Huang, F. Kondev, G. Audi, and S. Naimi, The AME 2020 atomic mass evaluation (II). Tables, graphs and references, Chin. Phys. C **45**, 030003 (2021).

[16] J. Dilling, P. Bricault, M. Smith, and H.-J. Kluge, The proposed TITAN facility at ISAC for very precise mass measurements on highly charged short-lived isotopes, Nucl. Instrum. Methods Phys. Res. B **204**, 492 (2003), Special issue, 14th International Conference on Electromagnetic Isotope Separators and Techniques Related to their Applications.

[17] S. Beck, B. Kootte, I. Dedes, T. Dickel, A. A. Kwiatkowski, E. M. Lykiardopoulou, W. R. Plaß, M. P. Reiter, C. Andreoiu, J. Bergmann, T. Brunner, D. Curien, J. Dilling, J. Dudek, E. Dunling, J. Flowerdew, A. Gaamouci, L. Graham, G. Gwinner, A. Jacobs *et al.*, Mass Measurements of Neutron-Deficient Yb Isotopes and Nuclear Structure at the Extreme Proton-Rich Side of the $N = 82$ Shell, Phys. Rev. Lett. **127**, 112501 (2021).

[18] C. Jesch, T. Dickel, W. Plaß, D. Short, S. S. Andres, J. Dilling, H. Geissel, F. Greiner, J. Lang, K. Leach, W. Lippert, C. Scheidenberger, and M. Yavor, The MR-TOF-MS isobar separator for the TITAN facility at TRIUMF, Hyperfine Interact. **235**, 97 (2015).

[19] M. Reiter, S. A. S. Andrés, J. Bergmann, T. Dickel, J. Dilling, A. Jacobs, A. Kwiatkowski, W. Plaß, C. Scheidenberger, D. Short, C. Will, C. Babcock, E. Dunling, A. Finlay, C. Hornung, C. Jesch, R. Klawitter, B. Kootte, D. Lascar, E. Leistenschneider *et al.*, Commissioning and performance of TITAN's multiple-reflection time-of-flight mass-spectrometer and isobar separator, Nucl. Instrum. Methods Phys. Res. A **1018**, 165823 (2021).

[20] W. Huang, G. Audi, M. Wang, F. G. Kondev, S. Naimi, and X. Xu, The AME2016 atomic mass evaluation (I). Evaluation of input data and adjustment procedures, Chin. Phys. C **41**, 030002 (2017).

[21] G. Audi, The evaluation of atomic masses, Hyperfine Interact. **132**, 7 (2001).

[22] M. Sandzelius, E. Ganioğlu, B. Cederwall, B. Hadinia, K. Andgren, T. Bäck, T. Grahn, P. Greenlees, U. Jakobsson, A. Johnson, P. M. Jones, R. Julin, S. Juutinen, S. Ketelhut, A. Khaplanov, M. Leino, M. Nyman, P. Peura, P. Rahkila, J. Sarén *et al.*, First observation of excited states in ^{172}Hg, Phys. Rev. C **79**, 064315 (2009).

[23] D. O'Donnell, R. D. Page, C. Scholey, L. Bianco, L. Capponi, R. J. Carroll, I. G. Darby, L. Donosa, M. Drummond, F. Ertuğral, T. Grahn, P. T. Greenlees, K. Hauschild, A. Herzan, U. Jakobsson, P. Jones, D. T. Joss, R. Julin, S. Juutinen, S. Ketelhut *et al.*, First observation of excited states of ^{173}Hg, Phys. Rev. C **85**, 054315 (2012).

[24] C. R. Bingham, K. S. Toth, J. C. Batchelder, D. J. Blumenthal, L. T. Brown, B. C. Busse, L. F. Conticchio, C. N. Davids, T. Davinson, D. J. Henderson, R. J. Irvine, D. Seweryniak, W. B. Walters, P. J. Woods, and B. E. Zimmerman, Identification of ^{166}Pt and ^{167}Pt, Phys. Rev. C **54**, R20 (1996).

[25] H. Kettunen, T. Enqvist, T. Grahn, P. T. Greenlees, P. Jones, R. Julin, S. Juutinen, A. Keenan, P. Kuusiniemi, M. Leino, A.-P. Leppänen, P. Nieminen, J. Pakarinen, P. Rahkila, and J. Uusitalo, Decay studies of ^{170,171}Au, $^{171-173}$Hg, and ^{176}Tl, Phys. Rev. C **69**, 054323 (2004).

[26] S. King, J. Simpson, R. Page, N. Amzal, T. Bäck, B. Cederwall, J. Cocks, D. Cullen, P. Greenlees, M. Harder, K. Helariutta, P. Jones, R. Julin, S. Juutinen, H. Kankaanpää, A. Keenan, H. Kettunen, P. Kuusiniemi, M. Leino, R. Lemmon *et al.*, First observation of excited states in the neutron deficient nuclei ^{168}Pt and ^{170}Pt, Phys. Lett. B **443**, 82 (1998).

[27] M. B. Gómez Hornillos, D. O'Donnell, J. Simpson, D. T. Joss, L. Bianco, B. Cederwall, T. Grahn, P. T. Greenlees, B. Hadinia, P. Jones, R. Julin, S. Juutinen, S. Ketelhut, M. Labiche, M. Leino, M. Nyman, R. D. Page, E. S. Paul, M. Petri, P. Peura *et al.*, γ-ray spectroscopy approaching the limits of existence of atomic nuclei: A study of the excited states of ^{168}Pt and ^{169}Pt, Phys. Rev. C **79**, 064314 (2009).

[28] A. N. Andreyev, S. Antalic, D. Ackermann, T. E. Cocolios, V. F. Comas, J. Elseviers, S. Franchoo, S. Heinz, J. A. Heredia, F. P. Heßberger, S. Hofmann, M. Huyse, J. Khuyagbaatar, I. Kojouharov, B. Kindler, B. Lommel, R. Mann, R. D. Page, S. Rinta-Antila, P. J. Sapple *et al.*, The new isotope ^{179}Pb and α-decay properties of ^{179}Tl^{m}, J. Phys. G: Nucl. Part. Phys. **37**, 035102 (2010).

[29] Mass Explorer, http://massexplorer.frib.msu.edu.

[30] J. P. Delaroche, M. Girod, J. Libert, H. Goutte, S. Hilaire, S. Péru, N. Pillet, and G. F. Bertsch, Structure of even-even nuclei using a mapped collective Hamiltonian and the D1SGogny interaction, Phys. Rev. C **81**, 014303 (2010).

[31] M. Bender, P.-H. Heenen, and P.-G. Reinhard, Self-consistent mean-field models for nuclear structure, Rev. Mod. Phys. **75**, 121 (2003).

[32] M. Kortelainen, J. McDonnell, W. Nazarewicz, P.-G. Reinhard, J. Sarich, N. Schunck, M. V. Stoitsov, and S. M. Wild, Nuclear energy density optimization: Large deformations, Phys. Rev. C **85**, 024304 (2012).

[33] J. Bartel, P. Quentin, M. Brack, C. Guet, and H.-B. Håkansson, Towards a better parametrisation of Skyrme-like effective forces: A critical study of the SKM force, Nucl. Phys. A **386**, 79 (1982).

[34] J. Dobaczewski, H. Flocard, and J. Treiner, Hartree-fock-bogolyubov description of nuclei near the neutron-drip line, Nucl. Phys. A **422**, 103 (1984).

[35] E. Chabanat, P. Bonche, P. Haensel, J. Meyer, and R. Schaeffer, A Skyrme parametrization from subnuclear to neutron star densities Part II. Nuclei far from stabilities, Nucl. Phys. A **635**, 231 (1998).

[36] P. Klüpfel, P.-G. Reinhard, T. J. Bürvenich, and J. A. Maruhn, Variations on a theme by Skyrme: A systematic study of adjustments of model parameters, Phys. Rev. C **79**, 034310 (2009).

[37] S. Seabold and J. Perktold, statsmodels: Econometric and statistical modeling with PYTHON, *9th PYTHON in Science Conference* (2010).

Correction: A typographical error in a value given in the fifth row of the second column of Table I has been fixed.